Quantum interference in two-photon frequency-comb spectroscopy

D. C. Yost,[1,*] A. Matveev,[1] E. Peters,[1,2] A. Beyer,[1] T. W. Hänsch,[1,2] and Th. Udem[1]

[1]*Max-Planck-Institut für Quantenoptik, 85748 Garching, Germany*
[2]*Ludwig-Maximilians-Universität, München, Fakultät für Physik, Schellingstrasse 4/III, 80799 München, Germany*

Quantum interference arising from spontaneous emission, or cross-damping, is an important yet frequently overlooked systematic in precision spectroscopy experiments which aim to determine a transition frequency with an uncertainty smaller than the natural linewidth. Here, we calculate the effects of such interference in two-photon frequency-comb spectroscopy using a perturbative approach and by integration of the density matrix equations. We then apply these techniques to the two-photon spectroscopy of the hydrogen $1S$-$3S$ transition currently being performed in our group. Depending on the detection geometry, we find distortions of the line shapes which can lead to systematic errors of $\sim$1 kHz if such interference effects are ignored in the data analysis. This result is independent of whether a cw laser or frequency comb is used for the excitation. Finally, we propose a time-dependent detection scheme which, when used in conjunction with frequency-comb excitation, can mitigate the line distortions arising from such interference.

PACS number(s): 32.70.Jz, 32.30.Jc, 32.10.Fn, 42.62.Fi

I. INTRODUCTION

High-precision spectroscopy of simple atomic systems offers the determination of fundamental constants and tests of quantum electrodynamics (QED) through comparison with accurate theoretical calculations. While such measurements have historically been very fruitful endeavors, they require the painstaking process of dutifully reducing or quantifying systematics to a level below the measurement uncertainty. Interestingly, several authors have recently identified that when two or more levels in an atomic system are closely spaced in energy, quantum interference manifested in spontaneous emission, commonly referred to as cross-damping, produces systematic line shifts which have often been overlooked [1–3]. Here, we analyze the effects of such interference in two-photon, frequency-comb spectroscopy. While this may appear to be a very specialized case on which to base our analysis, we anticipate that this form of spectroscopy will become increasingly important in the precision measurement of simple atomic and ionic systems as it offers broad spectral coverage and efficient harmonic conversion to short wavelengths [4–8]. Further, laser excitation with a continuous-wave (cw) source can easily be treated as a special case within our formalism.

In this article, we first present a review of the effects of quantum interference on the lifetimes of excited states, which is necessary to understand our later analysis. Then, in Sec. III, we derive an equation analogous to the Kramers-Heisenberg equation (see, for instance, [9,10]) using perturbation theory. A similar method has been used recently to calculate line distortions in ^{6,7}Li D_2 lines [3]. Our formulation differs from the traditional Kramers-Heisenberg formula in that it includes two-photon excitation by a frequency comb and velocity effects such as transit-time broadening. In Sec. IV, we analyze the line distortions that can be present in the measurements of the hydrogen $1S$-$3S$ transition, currently underway in our group and in the group of François Biraben in Paris [11–13], and check our results by a direct integration of the density

matrix equations [1,14]. Finally, in Sec. V we propose a detection scheme where a time-dependent detection window is applied to the fluorescence signal. This method can only be utilized in combination with frequency-comb excitation and mitigates the line-pulling effects that result from the quantum interference.

Our analysis is timely given the recent discrepancy between the determination of the proton charge radius through spectroscopy of muonic hydrogen versus regular hydrogen [15]. While the hydrogen $1S$-$2S$ transition has been determined with a very low fractional frequency uncertainty of 4.2×10^{-15} [16], it must be considered along with other less precisely determined transitions in hydrogen to extract the Rydberg constant and proton charge radius. To be relevant, these transitions must be measured to a small fraction of their natural linewidths and are therefore susceptible to the cross-damping systematic [17].

Our perturbative analysis is the focus of this article even though a direct integration of the density matrix equations is obviously more general. For instance, with direct integration, intensity-dependent effects, such as saturation and optical pumping, can also be taken into account. However, when dealing with a large number of relevant levels, the number of equations present in the density matrix treatment grows as the number of levels squared and is cumbersome to solve analytically. Obviously, such a system of equations can be numerically integrated, but physical insight may be lost. In contrast, the perturbative method retains the important features of the solution, is generally faster to implement, is less prone to computational errors, and can help guide our physical intuition. With this in mind, we make no attempt to avoid approximations to keep our perturbative results generally valid. Instead, we arrive at physically meaningful, simple expressions which, admittedly, should not be applied without caution to other precision spectroscopy experiments.

II. QUANTUM INTERFERENCE AND THE LIFETIMES OF EXCITED STATES

One predicted effect of quantum interference arising from spontaneous emission is a strong alteration of the lifetimes
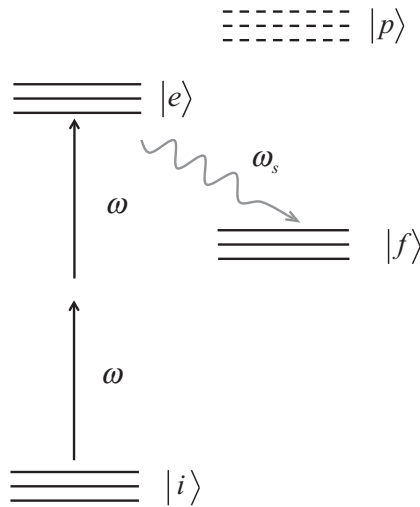
_____
*dylan.yost@mpq.mpg.de

FIG. 1. We consider two-photon excitation $(2 \times \omega)$ from initial states $|i\rangle$ through intermediate states $|p\rangle$ (far-off resonance) to excited levels $|e\rangle$. Excitation is detected through radiative decay at frequency ω_s to the final states $|f\rangle$. In principle, the manifold $|f\rangle$ may also decay back to the initial states, which is important to consider if optical pumping or saturation of the transition occurs.

of excited states [18]. These effects can, in principle, be so strong that they produce pseudometastable states if the proper excited-state coherences can be produced. However, this is often an artifact of restricting the analysis to a scalar atom without Zeeman structure. In a real atom, the dominant effect of the interference is the suppression of radiation in certain directions while enhancing it in others such that the overall excited-state lifetimes are maintained. The difficulty in achieving large alterations of excited-state lifetimes through the vacuum coupling in a real physical system has been discussed before [19–22]. However, we include a discussion here for clarity.

We first consider the master equation for the interaction of a multilevel atomic system with an electromagnetic field using the density matrix formalism [23,24].

$$\frac{\partial \rho}{\partial t} = \frac{1}{i\hbar}[H_I, \rho] - \mathcal{L}\rho. \quad (1)$$

We have grouped the decay terms in Eq. (1) into the Lindblad operator $\mathcal{L}$. We consider the general level structure shown in Fig. 1 which depicts two-photon excitation from a manifold of initial states $|i\rangle$ to a manifold of excited states $|e\rangle$ through the intermediate manifold $|p\rangle$. This is followed by spontaneous decay to a manifold of final states $|f\rangle$ through emission at frequency ω_s. Note that the manifolds could be partially or fully identical, for example, if the atom decays directly back to the initial states.

The decay terms from a particular excited state $|e'\rangle$ are given by $(\mathcal{L}\rho)_{e'e'}$, where we assume that state $|e'\rangle$ is part of the $|e\rangle$ manifold of states. Following from quantum electrodynamics and the Wigner-Weisskopf approximation, it can be shown that [21,22]

$$(\mathcal{L}\rho)_{e'e'} = \frac{1}{2} \sum_{ef\eta} \frac{D_{fe'}^{\eta} D_{fe}^{\eta} \omega_{ef}^3}{3\pi \epsilon_0 \hbar c^3} (\rho_{ee'} + \rho_{e'e}). \quad (2)$$

Here, we use the convention that $\omega_{ab} = (E_a - E_b)/\hbar$, and the dipole moments are given by $D_{fe}^{\eta} = q\langle f|\vec{\epsilon}_\eta \cdot \vec{r}|e\rangle$, where q is the elementary charge and $\vec{\epsilon}_\eta$ are the spherical unit vectors, expressed in Cartesian coordinates as $\vec{\epsilon}_0 = (0,0,1)$ and $\vec{\epsilon}_{\pm 1} = -(\pm 1, i, 0)/\sqrt{2}$ [25, Eq. (4.111)]. The spherical components $\eta = -1, 0, +1$ correspond respectively to σ_-, π, and σ_+ dipole radiation modes where the far-field electric field in the direction $\vec{R}$ is proportional to $(\vec{R} \times \vec{\epsilon}_\eta) \times \vec{R}$. From Eq. (2), we see that the decay of population from level $|e'\rangle$ depends not only on the population in $|e'\rangle$ (normal damping) but also on the coherence relative to other excited states $|e\rangle$ (cross-damping). For reference, please note that the full matrix $\mathcal{L}\rho$ is given later in the text [Eq. (23)].

We now show that when summing over all spherical components of dipole emission, the impact of cross-damping on the lifetimes is greatly reduced. Using the Wigner-Eckart theorem and the orthogonality relations of the Clebsch-Gordan coefficients, one finds that

$$\sum_{f\eta} D_{fe'}^{\eta} D_{fe}^{\eta} = 0, \quad (3)$$

unless states e and e' have the same angular momentum quantum numbers, differing only in principal quantum numbers. Typically, there will be no excited states near state $|e'\rangle$ which meet this condition, and therefore, Eq. (3) will hold unless $e = e'$. Due to the presence of the frequency ω_{ef}, we cannot directly apply the relationship given in Eq. (3) to Eq. (2). However, typically the level splitting between different angular momentum states in the manifold of states $|f\rangle$ is small compared to the absolute value of the frequencies ω_{ef}. Therefore, we find that

$$(\mathcal{L}\rho)_{e'e'} \approx \sum_{f\eta} \frac{\left(D_{fe'}^{\eta}\right)^2 \omega_{e'f}^3}{3\pi \epsilon_0 \hbar c^3} \rho_{e'e'} = \Gamma_{e'} \rho_{e'e'}, \quad (4)$$

where $\Gamma_{e'}$ is the decay rate of level $|e'\rangle$.

From Eq. (4), we find, with the caveats mentioned, that atomic levels will usually have well-defined total decay rates even in the presence of cross-damping. However, we do not claim that the cancellation given by Eq. (3) is perfect, only that the dominant effect of the quantum interference is to enhance a certain decay path while suppressing others such that the total decay rate is nearly constant. An examination of all approximations used in arriving at Eq. (4) is currently underway as small adjustments to the decay rates may be present which should be taken into account in more refined models [26]. One physical implication of well-defined lifetimes is that excitation dynamics should remain unaffected by cross-damping. Therefore, if one measures the excited-state population directly and optical pumping effects are negligible, cross-damping introduces no systematic effects.

There are special cases where the cross-damping would be expected to more significantly alter total decay rates. Artificial three-level systems could be created by the addition of coupling fields [18]. Also, by placing the atom in a cavity environment where certain decay channels are suppressed, it is expected that one can observe suppression of spontaneous decay from cross-damping effects [20]. Finally, Cardimona and Stroud [22] mention two systems where states differing only in principal quantum numbers can be close in frequency: Rydberg

atoms and multielectron atoms or molecules with overlapping electronic configurations. For such systems, Eq. (3) would no longer be applicable. With these precautions in mind, we assume well-defined lifetimes in our perturbative calculations in the next section.

III. PERTURBATIVE METHOD

A. Two-photon excitation and spontaneous emission

In this section, we analyze the excitation scheme shown in Fig. 1 using perturbation theory. For the case of Doppler-free two-photon spectroscopy, the atomic sample is probed with counterpropagating radiation and the first-order matrix elements from $|i\rangle$ to $|p\rangle$ are given by

$$c_{i \to p}^{(1)}(t) = \frac{c_i(0)}{i\hbar} \int_0^t \left[D_{pi}^{\nu} \mathcal{E}_+(t') + D_{pi}^{\mu} \mathcal{E}_-(t') \right] e^{i\omega_{pi}t'} dt'. \quad (5)$$

Here, $c_i(0)$ is the initial amplitude of state $|i\rangle$. We use $\mathcal{E}_{\pm}(t)$ to represent the amplitudes of the fields traveling in opposite directions and the labels ν and μ to denote their polarizations. We assume that all intermediate states labeled by $|p\rangle$ are far from laser resonance.

We now calculate the excited-state populations in the second order. In contrast to the first-order matrix elements, we anticipate that the levels $|e\rangle$ are close to resonance with the second harmonic of the field. Therefore, there will be significant population in the excited states, and we have to take into account the decay rates given by Γ_e. The use of well-defined decay rates was justified in the last section. However, such an inclusion appears here phenomenologically and depends upon the Wigner-Weisskopf theory of spontaneous emission. Therefore, such a treatment is, strictly speaking, beyond second-order perturbation theory.

$$c_{i \to e}^{(2)}(t) = \frac{c_i(0)}{(i\hbar)^2} \sum_p e^{-\frac{\Gamma_e}{2}t}$$

$$\times \int_0^t \int_0^{t'} \left[K(t',t'') + S(t',t'') \right]$$

$$\times e^{i(\omega_{pi}t'' + \omega_{ep}t') + \frac{\Gamma_e}{2}t'} dt'' dt'. \quad (6)$$

$K(t',t'')$ and $S(t',t'')$ are given by

$$K(t',t'') = D_{ep}^{\nu} D_{pi}^{\mu} \mathcal{E}_+(t') \mathcal{E}_-(t'') + D_{ep}^{\mu} D_{pi}^{\nu} \mathcal{E}_+(t'') \mathcal{E}_-(t'),$$

$$S(t',t'') = D_{ep}^{\nu} D_{pi}^{\nu} \mathcal{E}_+(t') \mathcal{E}_+(t'') + D_{ep}^{\mu} D_{pi}^{\mu} \mathcal{E}_-(t'') \mathcal{E}_-(t'). \quad (7)$$

For details on the proper inclusion of Γ_e in Eq. (6) see [9, Eqs. (2.181)–(2.186)]. The contribution from $K(t',t'')$ will produce the Doppler-free signal, whereas $S(t',t'')$ produces Doppler-broadened background. We ignore the $S(t',t'')$ term as it is relatively inconsequential for our results and discussion. However, it should be pointed out that under certain experimental conditions, the Doppler-broadened background can contribute significant shot noise and/or technical noise, and its suppression within a pulsed excitation scheme has been the subject of two recent articles [27,28].

Next, we take the two-dimensional Fourier transform of $K(t',t'')$ and evaluate the time integrals in Eq. (6). This

results in

$$c_{i \to e}^{(2)}(t) = c_i(0) \frac{Q_{ei}^{\mu\nu}}{2\pi\hbar} \int_{-\infty}^{\infty} \frac{\tilde{G}(\omega) e^{i(\omega_{ei}-2\omega)t}}{\omega_{ei} - 2\omega - i\frac{\Gamma_e}{2}} d\omega. \quad (8)$$

The function $\tilde{G}(\omega)$ is the Fourier transform of the product of the forward- and backward-propagating fields given by

$$\tilde{G}(\omega) = 2 \int_{-\infty}^{\infty} \mathcal{E}_+(t) \mathcal{E}_-(t) e^{i2\omega t} dt. \quad (9)$$

We also introduce a second-order dipole matrix element given by

$$Q_{ei}^{\mu\nu} = \sum_p \frac{D_{ep}^{\nu} D_{pi}^{\mu} + D_{ep}^{\mu} D_{pi}^{\nu}}{\hbar(\omega_{pi} - \omega_c)}. \quad (10)$$

Here, ω_c is the center frequency of the laser. Since we assume the denominator is far from resonance, the exact value of ω_c is not critical. For hydrogen, the second-order dipole matrix elements have been tabulated in [29].

Next, we must consider the radiative decay to the final state manifold $|f\rangle$. For this, we first calculate the amplitude that the atom decays by emitting a photon with frequency ω_s and in a dipole radiation pattern η. This is given by

$$c_{i \to f, \eta\omega_s}^{(3)}(t) = \frac{1}{i\hbar} \sum_e D_{fe}^{\eta} \int_0^t h_{\eta\omega_s} e^{i(\omega_s - \omega_{ef})t'} c_{i \to e}^{(2)}(t') dt'. \quad (11)$$

The quantity $h_{\eta\omega_s} = \sqrt{\hbar\omega_s/(2\epsilon_0 V)}$ can be thought of as the amplitude of the electric field per mode of the vacuum field in a given volume V, where we implicitly take the limit $V \to \infty$ later.

We can calculate the final population through $|c_{i \to f, \eta\omega_s}^{(3)}(t)|^2$, which is directly related to the photons scattered. In a typical experiment, there is not a precise measurement of the frequency of the emitted photon. Therefore, we include a density of states $dN/d\omega_s$ (proportional to V), integrate over ω_s, and sum over the initial and final states to find the emission intensity. This is given by

$$I^{\eta\mu\nu} = \sum_{if} \int_0^{\infty} \frac{dN}{d\omega_s'} \left| c_{i \to f, \eta\omega_s'}^{(3)}(t) \right|^2 d\omega_s'. \quad (12)$$

We now insert the result from Eq. (11) into Eq. (12) and take the limit $t \to \infty$, which corresponds physically to the total probability that the atom scattered a photon. For this limit to be physical, we must assume that the atom is excited only for some finite time, for example, an atom traveling through a laser beam. Evaluating the time integral in Eq. (11) gives

$$I^{\eta\mu\nu} = \frac{1}{4\hbar^4} \sum_{if} |c_i(0)|^2$$

$$\times \int_0^{\infty} \mathcal{H}(\omega_s') \left| \sum_e \frac{D_{fe}^{\eta} Q_{ei}^{\mu\nu} \tilde{G}\left[\frac{\omega_s' - \omega_{if}}{2}\right]}{\omega_{ef} - \omega_s' - i\frac{\Gamma_e}{2}} \right|^2 d\omega_s'. \quad (13)$$

In this equation, we introduce $\mathcal{H}(\omega_s) = \frac{dN}{d\omega_s} |h_{\eta\omega_s}|^2$, which will be proportional to ω_s^3 in free space and is independent of the volume V. In evaluating the time integral, we ignore the small contribution of the principal part as it is directly related

to the traditional Lamb shift, which can be better treated in more sophisticated models. Equation (13) is a function of the polarization of the excitation fields, ν and μ, and of the dipole radiation mode, η. We do not sum over η because an experimental measurement of fluorescence will often be preferentially sensitive to certain dipole radiation patterns.

As an aside, it may seem strange that Eq. (13) does not appear to display a two-photon resonance structure of the excited states $|e\rangle$. This is resolved if we consider a reasonable form for $\tilde{G}(\omega)$. For example, if we are exciting with a near-continuous-wave source, we would expect $\tilde{G}(\omega)$ to be strongly peaked around the carrier frequency ω_c. This will result in

$$I^{\eta\mu\nu} \propto \sum_{i\,f} \left| \sum_e \frac{D^\eta_{fe} Q^{\mu\nu}_{ei} \, \mathcal{H}(\omega_{ef})}{\omega_{ei} - 2\omega_c - i\frac{\Gamma_e}{2}} \right|^2. \tag{14}$$

This equation is the Kramers-Heisenberg formula except the usual single-photon matrix element has been replaced by a two-photon matrix element.

Returning to Eq. (13), we set $\mathcal{H}(\omega_s) = \mathcal{H}(\omega_{ef})$ and extend the integral to negative infinity, which is, in essence, the Wigner-Weisskopf approximation. We then use the method of partial fractions to rearrange Eq. (13) and arrive at

$$I^{\eta\mu\nu} = \frac{1}{2\hbar^4} \sum_{i\,f\,e\,e'} |c_i(0)|^2 \mathcal{H}(\omega_{ef})$$

$$\times \int_{-\infty}^{\infty} \mathrm{Re} \left[\frac{\mathcal{X}^{\eta\mu\nu}_{fe'ei} \left| \tilde{G}\left[\frac{\omega'_s - \omega_{if}}{2}\right] \right|^2}{\left(\omega_{e'e} - i\frac{\Gamma_e + \Gamma_{e'}}{2}\right)\left(\omega_{ef} - \omega'_s + i\frac{\Gamma_e}{2}\right)} \right] d\omega'_s, \tag{15}$$

where

$$\mathcal{X}^{\eta\mu\nu}_{fe'ei} = D^\eta_{fe} Q^{\mu\nu}_{ei} D^\eta_{fe'} Q^{\mu\nu}_{e'i}. \tag{16}$$

The latter expression represents a rather straightforward sum of products of $3j$ and $6j$ symbols [25, Eqs. (4.120), (4.175)] with the appropriate resonance denominator of Eq. (10). The quantum interference, represented in Eq. (15) by the terms in the sum where $e \neq e'$, can be understood as the interference between two quantum paths starting at state $|i\rangle$ and ending at state $|f\rangle$ through different excited states $|e\rangle$ and $|e'\rangle$.

B. Frequency-comb excitation of a moving atom

In this section, we consider the excitation of a moving atom by identical, counterpropagating frequency combs. We also assume the laser radiation has a Gaussian transverse-intensity profile and flat wave fronts and propagates along the x axis (see Fig. 2). This produces fields in the frame of the moving atom given by

$$\mathcal{E}_\pm(t) = \sum_{n=-\infty}^{\infty} \mathcal{E}_0 e^{-\frac{y(t)^2}{2w_y^2} - \frac{z(t)^2}{2w_z^2}} e^{-[t \mp x(t)/c - nt_r]^2/2\tau^2} e^{-i\,\omega_c(t \mp x(t)/c)}. \tag{17}$$

Here, the position of the atom is given by $\vec{r}(t) = [x(t), y(t), z(t)]$, t_r is the repetition period of the frequency comb, τ is the width of the pulses, and ω_c is the carrier frequency. We assume the pulses to be transform limited,
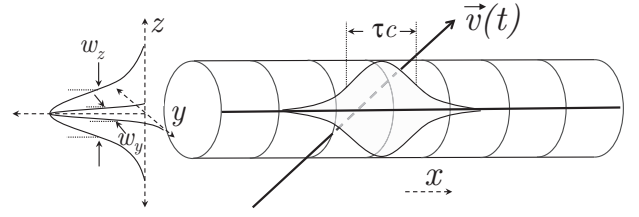

FIG. 2. Atomic trajectory passing through a Gaussian laser beam. We assume a linear trajectory which gives an atomic position of the form $\vec{r}(t) = [(x_0 + v_x t), (y_0 + v_y t), (z_0 + v_z t)]$. We also assume the laser beam has a Rayleigh range much larger than the beam waist so that its x dependence is negligible. A Doppler-free signal is obtained only from the pulse collision volume which is defined by the size of the beam waists in the transverse dimensions (w_y and w_z) and the length of the transform-limited, colliding pulses along the x axis (τc).

although the effects of spectral chirp can easily be included [27,28,30,31].

The dependence of the two-photon excitation on the applied laser fields is contained within the function $\tilde{G}(\omega)$ as defined by Eq. (9). By inserting Eq. (17) into Eq. (9) we arrive at

$$\tilde{G}(\omega) = \mathcal{E}_0^2 \sum_{n=-\infty}^{\infty} \int_{-\infty}^{\infty} e^{-\frac{x(t)^2}{\tau^2 c^2} - \frac{y(t)^2}{w_y^2} - \frac{z(t)^2}{w_z^2}}$$

$$\times e^{-(t - nt_r)^2/\tau^2} e^{-2i\omega_c t} e^{i2\omega t} dt. \tag{18}$$

The first factor describes the rising and falling intensity that the atom experiences as it travels across the pulse-collision volume, whereas the second factor describes the time dependence of the pulse trains themselves.

We now assume a linear trajectory, $\vec{r}(t) = [(x_0 + v_x t), (y_0 + v_y t), (z_0 + v_z t)]$, and evaluate the Fourier transform represented in Eq. (18). This gives

$$\tilde{G}(\omega) \propto \sum_{q=-\infty}^{\infty} e^{-\frac{(q - 2q_c)^2 \omega_r^2 \tau^2}{4}} e^{-\frac{(2\omega - 2\omega_0 - q\omega_r)^2 t_\delta^2}{4}} e^{i\phi_q(\omega)}. \tag{19}$$

Here, $\omega_r = 2\pi/t_r$ and $\omega_0 = \omega_c - q_c \omega_r$ are the repetition and offset frequencies of the fundamental frequency combs [32], q_c is the mode number nearest the center of the spectrum, and $t_\delta = (v_x^2/c^2\tau^2 + v_y^2/w_y^2 + v_z^2/w_z^2)^{-\frac{1}{2}}$ is the time it takes the atom to traverse the pulse collision volume. The phase $\phi_q(\omega) = [2\omega - 2\omega_c - (q - 2q_c)\omega_r]t_0$ usually drops out of the calculation, as we show later.

For the total scattering amplitude as given in Eq. (15), we must calculate $|G(\omega)|^2$, which is given by

$$|\tilde{G}(\omega)|^2 \propto \sum_{q,p=-\infty}^{\infty} e^{i[\phi_q(\omega) - \phi_p(\omega)]} e^{-\frac{(q - 2q_c)^2 \omega_r^2 \tau^2}{4} - \frac{(p - 2q_c)^2 \omega_r^2 \tau^2}{4}}$$

$$\times e^{-\frac{(2\omega - 2\omega_0 - q\omega_r)^2 t_\delta^2}{4} - \frac{(2\omega - 2\omega_0 - q\omega_r)^2 t_\delta^2}{4}}. \tag{20}$$

We can usually ignore terms where $p \neq q$. The validity of this depends on the frequency-comb modes being relatively well separated. For instance, if $t_\delta \sim 200$ ns and $\omega_r \sim 1$ GHz, then terms with $p \neq q$ will be approximately e^{-100^2} times the terms with $p = q$. By setting terms where $p \neq q$ to zero, the dependence on the spectral phases $\phi_q(\omega)$ and $\phi_p(\omega)$ cancels,

and Eq. (20) simplifies to

$$|\tilde{G}(\omega)|^2 \propto \sum_{q=-\infty}^{\infty} e^{-\frac{(q-2q_c)^2\omega_r^2\tau^2}{2}} e^{-\frac{(2\omega-2\omega_0-q\omega_r)^2 t_\delta^2}{2}}. \tag{21}$$

We insert this result into Eq. (15) and define a new variable of integration, $\xi = \omega'_s - \omega_{if} - 2\omega_0 - q\omega_r$.

$$I^{\eta\mu\nu} \propto \sum_{q=-\infty}^{\infty} |c_i(0)|^2 e^{-\frac{(q-2q_c)^2\omega_r^2\tau^2}{2}} \sum_{ifee'} \mathcal{X}_{fe'ei}^{\eta\mu\nu} \mathcal{H}(\omega_{ef})$$

$$\times \int_{-\infty}^{\infty} \mathrm{Re}\left[\frac{e^{-\frac{\xi^2 t_\delta^2}{2}}}{\left(\omega_{e'e} - i\frac{\Gamma_e + \Gamma_{e'}}{2}\right)\left(\omega_{ei} - 2\omega_0 - \omega_r q - \xi + i\frac{\Gamma_e}{2}\right)} \right] d\xi. \tag{22}$$

Equation (22) is our final result, which we use to analyze the measurement of the hydrogen 1S-3S transition.

One of the main strengths of Eq. (22) is that it is easily interpreted. Terms in the sum with $e' \neq e$ describe the quantum interference and will be suppressed by roughly $\omega_{e'e}/\Gamma_e$ when compared with terms with $e' = e$, provided the level splitting in the $|e\rangle$ manifold is larger than the natural linewidths. The leading exponent describes the spectral shape of the second harmonic of the frequency comb and shows that a transition will be excited more efficiently if it is well centered within this spectrum. The integral over ξ is necessary to include line-broadening mechanisms. However, if these effects are small compared to the natural linewidth, then ξ can be set to zero in the denominator, and the integral can easily be evaluated. $\mathcal{H}(\omega_{ef})$ will be proportional to ω_{ef}^3 in free space, and it can usually be ignored provided that splittings between levels within the $|e\rangle$ and $|f\rangle$ manifolds are small.

As mentioned above, Eq. (22) reveals that the effects of cross-damping are generally proportional to $1/\omega_{e'e}$ as long as the level splittings are much larger than the natural width. This deserves special mention because, intuitively, one might expect that since two widely separated levels can easily be put into a coherent superposition when excited by a frequency comb, the relevant proportionality constant would be $1/(\omega_{e'e} \bmod \omega_r)$, which is evidently not the case. Practically, this shows that we are not introducing larger cross-damping effects by using frequency-comb spectroscopy instead of cw laser spectroscopy. The case of cw excitation can be treated as a special case of Eq. (22) by considering only the term $q = 0$ in the sum.

IV. APPLICATION TO HYDROGEN 1S-3S SPECTROSCOPY AND COMPARISON WITH NUMERICAL INTEGRATION OF THE DENSITY MATRIX EQUATIONS

In this section we apply Eq. (22) to spectroscopy of the hydrogen 1S-3S transition. Figure 3 shows the relevant levels. The 3S and 3D levels have natural linewidths of 1.0 and 10.3 MHz, respectively. We consider both the 3D and 3S levels as part of the $|e\rangle$ manifold. Figure 4 shows the detected signal we expect as we scan ω_0. The counterpropagating beams have polarization $\nu = \mu = 0$ (linear polarization along

the z axis) and a repetition rate of 348.16 MHz. Figure 4 also shows the residual errors if we leave out the terms in Eq. (22) where $e \neq e'$, which is equivalent to ignoring the quantum interference. These errors are dependent on which dipole emission components ($\sigma_\pm$ or π) are detected. In a typical experimental setup, it is usually some combination of emission patterns which is measured, which depends on the placement and polarization sensitivity of the detector. Figure 5 shows the line shifts which result from fitting the distorted lines with Lorentzians as a function of detector placement. Figure 5 also shows a comparison with the case of cw excitation. As is evident in Fig. 5 and discussed in Sec. III, the combination of frequency-comb excitation and the quantum interference does not introduce additional systematic effects, so that the curves are nearly identical.

Figure 6 shows the detected signal and residuals if the line is broadened through a 10 times smaller t_δ. In this case,
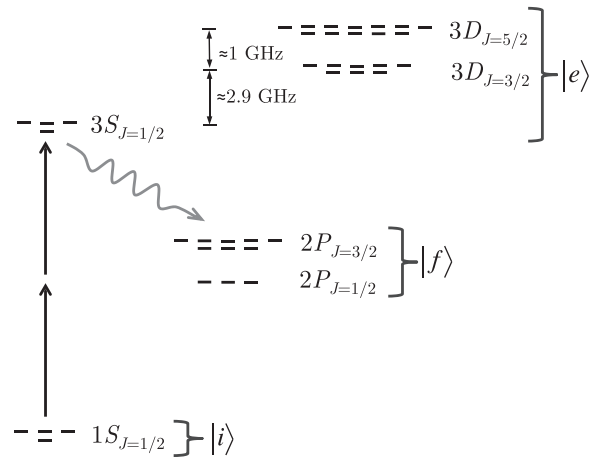

FIG. 3. Relevant hydrogen levels with all hyperfine levels shown. The m_F levels of the same F are shown as horizontally displaced. We model the excitation of the allowed two-photon 1S-3S transitions ($F = 0$ to $F = 0$ and $F = 1$ to $F = 1$) using counterpropagating beams of π polarization. To compare with Fig. 1, all 3S and 3D levels comprise the $|e\rangle$ manifold, the 2P levels comprise the $|f\rangle$ manifold, and the 1S levels comprise the $|i\rangle$ manifold. The $|p\rangle$ manifold (not shown) is all levels that are dipole allowed from the 1S level.
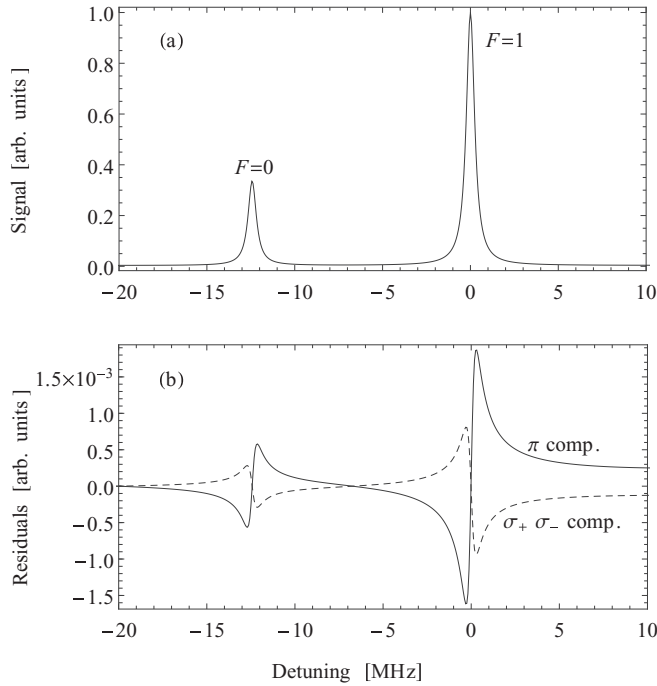
FIG. 4. (a) Calculated fluorescence signal from the $3S$ levels using Eq. (22) as the offset frequency ω_0 is scanned with $t_\delta = 2$ μs and a repetition rate of $\omega_r = 2\pi \times 348.16$ MHz. The repetition rate is chosen so that only the $3S$ levels are resonantly excited within the scan range shown. Since we show frequency-comb excitation, the $F = 0$ and $F = 1$ transitions appear closely spaced but are actually excited by separate comb modes. (b) Difference in the line shape between the full model and when only terms where $e = e'$ are considered in Eq. (22) [note that the units in (b) are arbitrary, but the same as the units in (a)]. The errors depend on the detected dipole spherical components and average to zero if they are all detected with equal sensitivity. The σ_+ and σ_- components are identical and are shown as the dashed line.
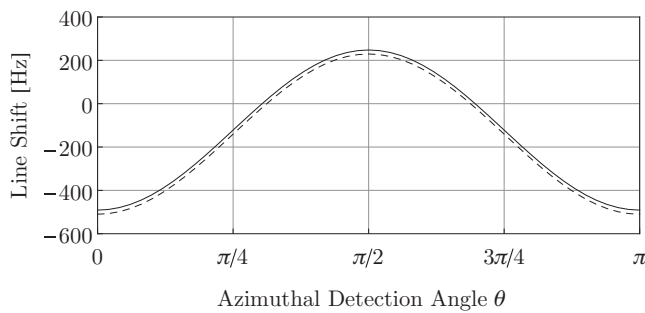

FIG. 5. The line-center shift of the $1S$ $F = 1$ to $3S$ $F = 1$ transition which results from fitting the line profiles distorted by quantum interference with Lorentzian functions. We assume a small-area detector which detects a combination of the π and $\sigma_\pm$ dipole spherical components with a laser polarization of $\mu = \nu = 0$ (both beams linearly polarized along the z axis). In this case, there is cylindrical symmetry, so we plot the result only as a function of the azimuthal angle θ (with respect to the z axis). The solid and dashed lines represent the frequency-comb and cw excitation cases, respectively. Note that the shifts shown correspond to a $\sim 10^{-13}$ relative frequency error for the spectroscopic measurement.
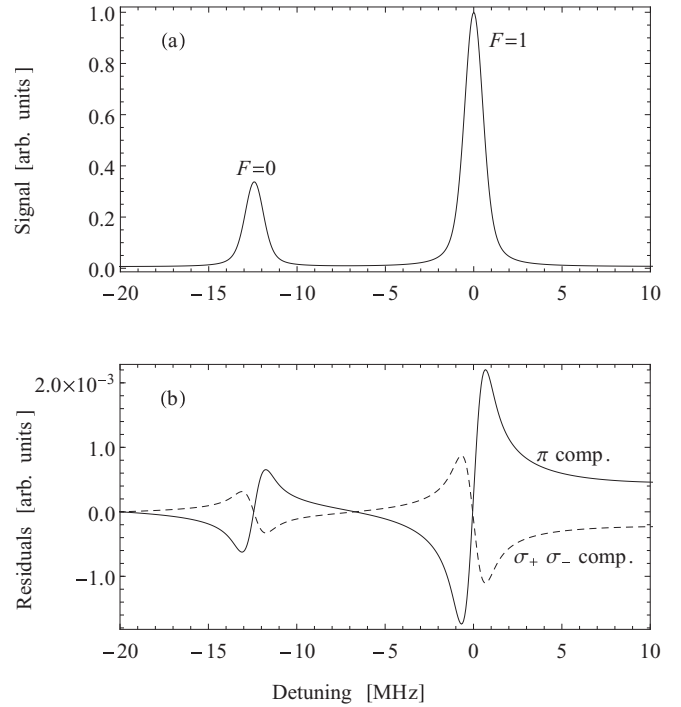

FIG. 6. Similar to Fig. 4 with only the $1S$-$3S$ transitions resonantly excited within the scan range shown. The transit time broadening is no longer negligible ($t_\delta = 200$ ns), and therefore, the residual errors in (b) broaden and are proportionally larger than in Fig. 4.

the residuals are proportionally larger and also broadened. From this result, it is clear that the combination of transit-time broadening and cross-damping cannot be treated as unrelated systematic effects and must be considered together.

We can compare our results obtained with our perturbative formulation with a direct numerical integration of the density matrix equations in Eq. (1). For this, we require the full Lindblad operator $\mathcal{L}$, approximated by [23,24]

$$\mathcal{L}\rho = \frac{1}{2} \sum_{ij} \gamma_{ij} \{ S_i^+ S_j^- \rho - 2 S_j^- \rho S_i^+ + \rho S_i^+ S_j^- \}. \quad (23)$$

Here, the indices i and j label transitions and not levels, and ω_i is the corresponding frequency for that transition. The cross-damping coefficients are given by $\gamma_{ij} = \sqrt{\gamma_i \gamma_j} \, \vec{\epsilon}_i \cdot \vec{\epsilon}_j$, where γ_i are the decay constants for transition i and $\vec{\epsilon}_i$ are the spherical unit vectors along the corresponding dipole moments. The operator S_i^+ is given by $|e\rangle\langle f|$, where states e and f are levels which correspond to transition i. Likewise, S_i^- is given by $|f\rangle\langle e|$. As can be seen in Fig. 3, there are 39 levels which should be accounted for in our analysis. For the case of linearly polarized excitation beams the $3D$ magnetic sublevels with $m_F = \pm 3, \pm 2$ cannot be excited because of two-photon selection rules, which leaves 32 quantum states. The total number of equations represented by Eq. (1) is therefore $32^2 = 1024$.

To obtain the fluorescence signal from the $3S/3D$-$2P$ decay in the simulation, we determine the transfer of population from the manifolds $|e\rangle$ to $|f\rangle$, along with the required radiated
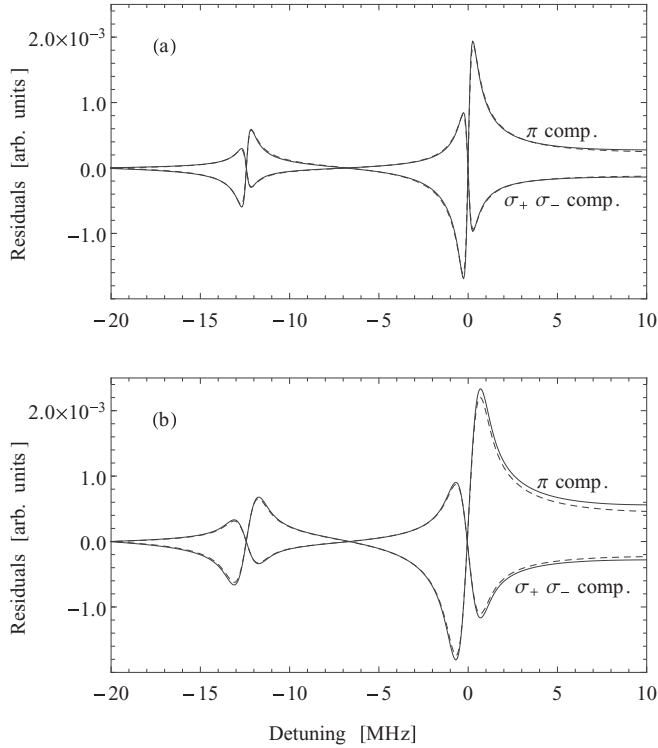
FIG. 7. Difference between the calculated line shapes when integrating the complete set of density matrix equations and when we set $\gamma_{ij} = 0$ if $i \neq j$ (equivalent to ignoring the cross-damping). The dashed curves are reproduced from the perturbative calculations shown in Figs. 4 and 6 so that the two methods can be compared. In (a) $t_\delta = 2\ \mu$s, and in (b) $t_\delta = 200$ ns.

spherical component ($\sigma_\pm$ or π) for the transition. To simulate the evolution of a hydrogen atom flying through the laser field, we must integrate 1024 equations.

Figure 7 shows a comparison of the residuals calculated through the perturbative method and through an integration of the density matrix equations. As is evident from Fig. 7, the two techniques produce nearly identical line distortions. While our perturbative approach is simpler to implement and intuitive, the density matrix approach is able to model saturation effects, which depend on the intensity of the counterpropagating laser beams. However, we found that when using beams with 1 kW of average power, optical pumping effects contributed less than 1% to the residuals shown in Fig. 7. In the experiment, the average power we use for excitation is less than 100 mW [13].

One can observe from Fig. 7 that if all radiated polarizations are detected with equal probability, the line-pulling effects of quantum interference vanish because the distortions observed when detecting the $\sigma_\pm$ radiated polarizations are one-half the magnitude and opposite in sign to the distortions when detecting the π polarization. This property is intuitive since the detection of all fluorescence regardless of polarization or dipole-emission pattern results in a pure measurement of the population in the excited states and, as discussed in Sec. II, such a measurement is unaffected by cross-damping given a few caveats.

V. TIME-DEPENDENT DETECTION

In this section, we analyze the temporal dynamics of the quantum interference when our system is excited with counterpropagating, coherent pulse trains (i.e., frequency combs). We find that the line distortions can often be mitigated if we detect only the fluorescence that is emitted between pulses in the train. To illustrate this effect, we first consider only two time-dependent radiating dipoles $d_S(t)$ and $d_D(t)$ between two separate excited states in the $|e\rangle$ manifold but sharing the same final state in the $|f\rangle$ manifold.

In keeping with our previous discussion, we assume an atom which has nonzero velocity and travels across a pulsed laser beam with a Gaussian transverse intensity profile. It will therefore experience a train of pulses with a rising and falling intensity. The effects of cross-damping on the fluorescence rate will be proportional to the cross term $2\,\mathrm{Re}\{d_S(t)d_D^*(t)\}$. The physical behavior of this term can be understood intuitively. When the atom is being driven by the laser field (i.e., when the a pulse is at the position of the atom), both dipole moments oscillate with the same frequency ($\omega_c - \omega_{fi}$). Between the pulses, these dipole moments oscillate with their distinct eigenfrequencies such that the resulting quantum beats average quickly to zero. This behavior is illustrated in Fig. 8 and is reminiscent of two classical oscillators which respond at the drive frequency when driven and at their respective resonant frequencies otherwise. The influence of the cross-damping on the signal will be proportional to $2 \int \mathrm{Re}\{d_S(t)d_D^*(t)\}dt$, and as

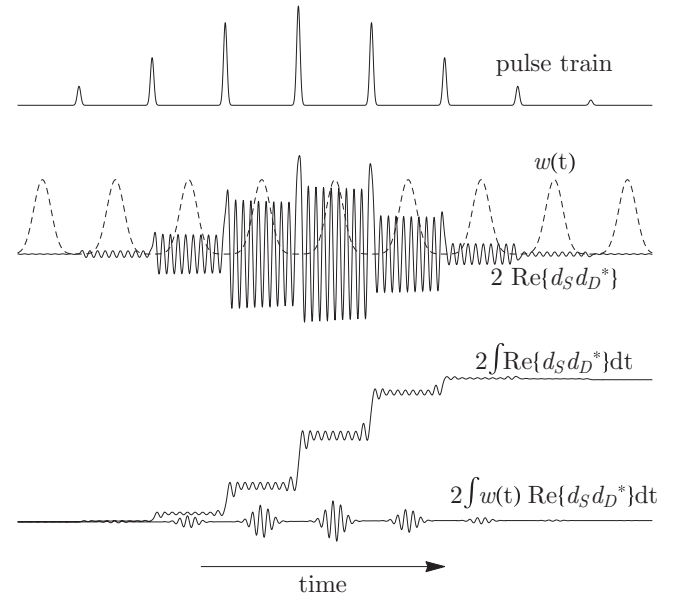FIG. 8. Illustration of the interference between the time-dependent dipoles [$2\,\mathrm{Re}\{d_S(t)d_D^*(t)\}$]. The rising and falling intensity of the pulses is because the atom has nonzero velocity and travels across a Gaussian laser beam. The additional signal which arises from this interference is proportional to the time integral of this interference [$2 \int \mathrm{Re}\{d_S(t)d_D^*(t)\}dt$]. This integral only accumulates when the pulse is at the position of the atom, and therefore, when applying an appropriate window function, $w(t)$, to the detected signal, the integral [$2 \int w(t)\mathrm{Re}\{d_S(t)d_D^*(t)\}dt$] is greatly reduced, mitigating the distortion.
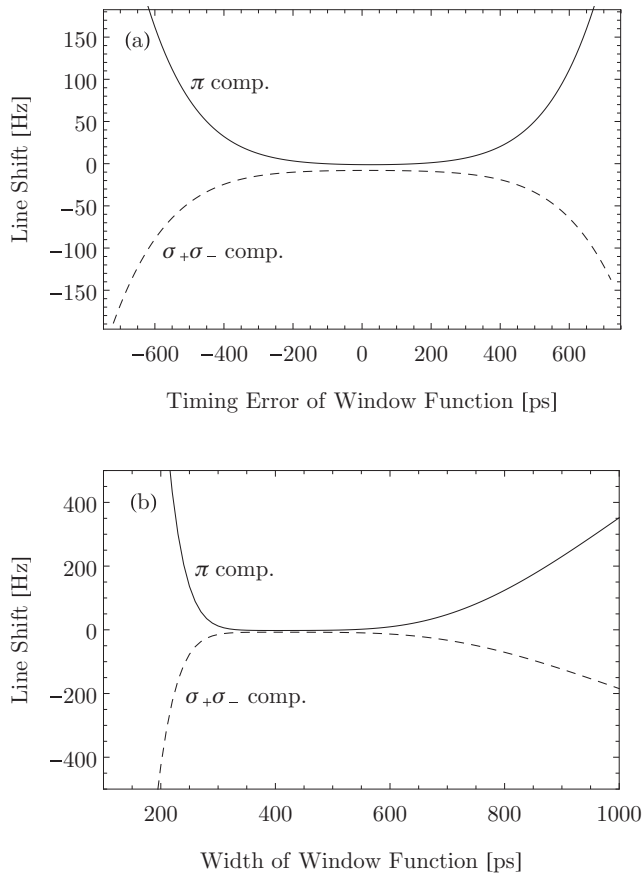
FIG. 9. Line center shift when the $1S$ $F = 1$ to $3S$ $F = 1$ transition is excited and detection of fluorescence is made through radiative decay to the $2P$ states after excitation by a 348.16-MHz repetition rate frequency comb with 1-ps pulses. A Gaussian window function is used to gate the detection between the pulses. (a) Line centers obtained from fitting a Lorentzian as a function of the timing of a Gaussian window function with a width of 500 ps. (b) Same as (a), but as a function of the width of the Gaussian window function.

can be seen in Fig. 8, the integral only accumulates when the atom is being driven by the laser field as one would expect. In between pulses, $2\mathrm{Re}\{d_S(t)d_D^*(t)\}$ predictably oscillates with zero mean. Therefore, if one detects the fluorescence only during times between pulses, the line distortion can be greatly mitigated.

A Gaussian window function $w(t)$ may be used to smoothly select the signal between the pulses. Of course, the window width cannot be larger than the repetition period but should contain at least several oscillations of the quantity $2\mathrm{Re}\{d_S(t)d_D^*(t)\}$, so that the average will approach zero.

This introduces the constraint that there must be at least several comb modes between the measured level and the perturbing level for the technique to be advantageous. The exact level of suppression of interference effects will depend on the position, width, and shape of the window function. For instance, it is necessary that $w(t)$ is turned on and off slowly when compared with the oscillation of $2\mathrm{Re}\{d_S(t)d_D^*(t)\}$ to prevent residual errors.

As a concrete example, we have used the density matrix approach to calculate the effects of the time-dependent detection scheme on the hydrogen $1S$-$3S$ transition with cross-damping effects from the $3D$ levels. In Fig. 9, we show the fitted line centers when using a Gaussian-shaped window function for photodetection. From Fig. 9, it is evident that there is a significant mitigation of the line-center shift when the window function position and width are chosen correctly. We also calculate the result as a function of the width and position of the Gaussian window and find that the sensitivity to these parameters is small when one considers the timing precision that can be obtained from typical laboratory electronics.

VI. CONCLUSION

The first part of the paper analyzed the effects of quantum interference on two-photon frequency-comb spectroscopy of the hydrogen $1S$-$3S$ transition through two distinct methods: a perturbative calculation and the integration of the density matrix equations. The agreement between our two different approaches gives us confidence that we are producing accurate line-shape models and that our assumption of well-defined excited state lifetimes is well founded. We find that, if such interference effects are ignored in the data analysis, the extracted frequencies can be shifted by ~1 kHz depending on the detection geometry. We can, of course, take these effects into account in the data analysis, which substantially reduces such systematic errors. Additionally, we have proposed an experimental method which can greatly mitigate the line distortions by applying a time-window function to the fluorescence. Such a scheme may be useful because we would not rely on theoretical corrections of our measured result.

[1] M. Horbatsch and E. A. Hessels, Phys. Rev. A **82**, 052519 (2010).

[2] M. Horbatsch and E. A. Hessels, Phys. Rev. A **84**, 032508 (2011).

[3] R. C. Brown, S. Wu, J. V. Porto, C. J. Sansonetti, C. E. Simien, S. M. Brewer, J. N. Tan, and J. D. Gillaspy, Phys. Rev. A **87**, 032504 (2013).

[4] M. Herrmann *et al.*, Phys. Rev. A **79**, 052505 (2009).

[5] E. E. Eyler, D. E. Chieda, M. C. Stowe, M. J. Thorpe, T. R. Schibli, and J. Ye, Eur. Phys. J. D **48**, 43 (2008).

[6] D. Z. Kandula, C. Gohle, T. J. Pinkert, W. Ubachs, and K. S. E. Eikema, Phys. Rev. Lett. **105**, 063001 (2010).

[7] S. Witte, R. T. Zinkstok, W. Ubachs, W. Hogervorst, and K. S. E. Eikema, Science **307**, 400 (2005).

[8] A. Cingöz, D. C. Yost, T. K. Allison, A. Ruehl, M. E. Fermann, I. Hartl, and J. Ye, Nature (London) **482**, 68 (2012).

[9] J. J. Sakurai, *Advanced Quantum Mechanics* (Addison-Wesley, Boston, 1967).

[10] R. Loudon, *The Quantum Theory of Light* (Oxford University Press, Oxford, 2000).

[11] O. Arnoult, F. Nez, L. Julien, and F. Biraben, Eur. Phys. J. D **60**, 243 (2010).

[12] S. Galtier, F. Nez, L. Julien, and F. Biraben, Opt. Commun. **324**, 34 (2014).

[13] E. Peters, D. C. Yost, A. Matveev, T. W. Hänsch, and T. Udem, Ann. Phys. (NY) **525**, L29 (2013).

[14] A. Marsman, M. Horbatsch, and E. A. Hessels, Phys. Rev. A **86**, 040501(R) (2012).

[15] R. Pohl *et al.*, Nature (London) **466**, 213 (2010).

[16] C. G. Parthey *et al.*, Phys. Rev. Lett. **107**, 203001 (2011).

[17] A. Beyer *et al.*, J. Phys. Conf. Ser. **467**, 012003 (2013).

[18] S.-Y. Zhu and M. O. Scully, Phys. Rev. Lett. **76**, 388 (1996).

[19] P. R. Berman, Phys. Rev. A **58**, 4886 (1998).

[20] A. K. Patnaik and G. S. Agarwal, Phys. Rev. A **59**, 3015 (1999).

[21] D. A. Cardimona, M. G. Raymer, and C. R. Stroud, Jr., J. Phys. B **15**, 55 (1982).

[22] D. A. Cardimona and C. R. Stroud, Jr., Phys. Rev. A **27**, 2456 (1983).

[23] G. S. Agarwal, in *Quantum Statistical Theories of Spontaneous Emission and Their Relation to Other Approaches*, edited by G. Möhler *et al.*, Springer Tracts in Modern Physics: Quantum Optics Vol. 70 (Springer, Berlin, 1974).

[24] Z. Ficek and S. Swain, *Quantum Interference and Coherence* (Springer, Berlin, 2005).

[25] I. Sobelman, *Atomic Spectra and Radiative Transitions* (Springer, Berlin, 1979).

[26] G. Morigi (private communication).

[27] I. Barmes, S. Witte, and K. S. E. Eikema, Phys. Rev. Lett. **111**, 023007 (2013).

[28] A. Ozawa and Y. Kobayashi, Phys. Rev. A **86**, 022514 (2012).

[29] M. Haas *et al.*, Phys. Rev. A **73**, 052501 (2006).

[30] E. Peters, S. A. Diddams, P. Fendel, S. Reinhardt, T. W. Hänsch, and Th. Udem, Opt. Express **17**, 9183 (2009).

[31] S. Reinhardt, E. Peters, T. W. Hänsch, and Th. Udem, Phys. Rev. A **81**, 033427 (2010).

[32] Th. Udem, R. Holzwarth, and T. W. Hänsch, Nature (London) **416**, 233 (2002).